Bond-order-modulated staggered-flux phase of the *tJ* model on a square lattice

Cédric Weber,[1] Didier Poilblanc,[2,3,*] Sylvain Capponi,[2] Frédéric Mila,[3] and Cyril Jaudet[2]

[1]*Institut Romand de Recherche Numérique en Physique des Matériaux (IRRMA), PPH-Ecublens, CH-1015 Lausanne, Switzerland*
[2]*Laboratoire de Physique Théorique UMR 5152, C.N.R.S. & Université de Toulouse, F-31062 Toulouse, France*
[3]*Institute of Theoretical Physics, Ecole Polytechnique Fédérale de Lausanne, BSP 720, CH-1015 Lausanne, Switzerland*

Motivated by the observation of inhomogeneous patterns in some high-T_c cuprate compounds, several variational Gutzwiller-projected wave functions with built-in charge and bond-order parameters are proposed for the extended *t-J-V* model on the square lattice at low doping. First, following a recent Gutzwiller-projected mean-field approach by one of us [D. Poilblanc, Phys. Rev. B **72**, 060508(R) (2005)], we investigate, as a function of doping and Coulomb repulsion the relative stability of a wide variety of modulated structures with square unit cells of size 2×2, $\sqrt{8} \times \sqrt{8}$, 4×4, and $\sqrt{32} \times \sqrt{32}$. It is found that the 4×4 bond-order wave function with staggered-flux pattern (and small charge and spin current density wave) is a remarkable competitive candidate for hole doping around 1/8 in agreement with scanning tunneling microscopy observations in the underdoped regime of some cuprates. This wave function is then optimized accurately and its properties studied extensively using a variational Monte Carlo scheme. Moreover, we find that under increasing the Coulomb repulsion, the *d*-wave superconducting RVB wave function is rapidly destabilized with respect to the 4×4 bond-order wave function. The stability of the bond-modulated wave function is connected to a gain of Coulomb and exchange energies. We suggest that such ordering patterns could be dynamical or could spontaneously appear in the vicinity of an impurity or a vortex in the mixed phase of the cuprates. Finally, we consider also a commensurate flux phase, but this wave function turns out *not* to be competitive because of its rather poor kinetic energy. However, we find it has very competitive exchange and Coulomb energies.

I. INTRODUCTION: MODELS AND METHODS

The observation of a *d*-wave superconducting gap in the high-T_c cuprate superconductors suggests[1] that strong correlations are responsible for their unconventional properties and superconducting behavior. The two-dimensional (2D) *t-J* model is one of the simplest effective models proposed[2] to describe the low-energy physics of these materials,

$$H_{t\text{-}J} = -t \sum_{\langle i,j \rangle, \sigma} (c_{i,\sigma}^{\dagger} c_{j,\sigma} + \text{H.c.}) + J \sum_{\langle i,j \rangle} \mathbf{S}_i \cdot \mathbf{S}_j. \quad (1)$$

The electrons are hopping between nearest-neighbor sites of a square lattice leading to a kinetic energy term (first term of 1) as well as an exchange energy due to their spin interaction (second term), where $\mathbf{S}_i$ denotes the spin at site *i*: $\mathbf{S}_i = \frac{1}{2} c_{i,\alpha}^{\dagger} \vec{\sigma}_{\alpha,\beta} c_{i,\beta}$ and $\vec{\sigma}$ is the vector of Pauli matrices. $\langle i,j \rangle$ stands for a pair of nearest neighbors. $H_{t\text{-}J}$ operates only in the subspace where there are no doubly occupied sites, which can be formally implemented by a Gutzwiller projector (see later). In the following we set $|t|=1$ (unless specified otherwise) and we adopt a generic value of $t/J=3$ throughout the paper. Because of the particle-hole symmetry in the square lattice the sign of *t* does not play any role. Although this model is formulated in a very simple form, the nature of the quantum correlations makes its physics very rich, and even the ground state of the *t-J* Hamiltonian was not yet characterized for finite doping and large cluster size. However, the *t-J* model was investigated extensively by unbiased numerical techniques[3] as well as by mean-field[4] and variational Monte Carlo approaches.[5,6] All approaches found a *d*-wave superconducting phase and a phase diagram which accounts for most of the experimental features of the high-T_c

cuprates.[7,8] In the limit of vanishing doping (half filling), such a state can be viewed as an (insulating) resonating valence bond (RVB) or *spin-liquid* state. In fact, such a state can also be written (after a simple gauge transformation) as a staggered flux state (SFP),[4,9] i.e., can be mapped to a problem of free fermions hopping on a square lattice thread by a staggered magnetic field.

Upon finite doping, although such a degeneracy breaks down, the SFP remains a competitive (nonsuperconducting) candidate with respect to the *d*-wave RVB superconductor.[10] In fact, it was proposed by P. A. Lee and collaborators[11–13] that such a state bears many of the unconventional properties of the pseudogap *normal* phase of the cuprate superconductors. This simple mapping connecting a free fermion problem on a square lattice under magnetic field[14] to a correlated wave function (see later for details) also enabled us to construct more exotic flux states (named as *commensurate flux states*) where the fictitious flux could be uniform and commensurate with the particle density.[15,16] In this particular case, the unit cell of the tight-binding problem is directly related to the rational value of the commensurate flux.

With an increasing number of materials and novel experimental techniques of constantly improving resolution, novel features in the global phase diagram of high-T_c cuprate superconductors have emerged. One of the most striking is the observation, in some systems, of a form of local electronic ordering, especially around 1/8 hole doping. Indeed, recent scanning tunneling microscopy/spectroscopy (STM/STS) experiments of underdoped $Bi_2Sr_2CaCu_2O_{8+\delta}$ (BSCO) in the pseudogap state have shown evidence of *energy-independent* real-space modulations of the low-energy density of states (DOS),[17–20] with a spatial period close to four lattice spacings. A similar spatial variation of the electronic states

has also been observed in the pseudogap phase of $Ca_{2-x}Na_xCuO_2Cl_2$ single crystals ($x=0.08-0.12$) by similar STM/STS techniques.[21] Although it is not clear yet whether such phenomena are either generic features or really happening in the bulk of the system, they, nevertheless, raise important theoretical questions about the stability of such structures in the framework of our microscopic strongly correlated models.

In this paper, we analyze the stability and the properties of different inhomogeneous phases (which may compete in certain conditions with the *d*-wave superconducting RVB state) by extending the previous mean-field and variational treatments of the RVB theory. In addition, we shall also consider an extension of the simple *t-J* model, the *t-J-V* model, containing a Coulomb repulsion term written as

$$V = \frac{1}{2}\sum_{i\neq j} V(|i-j|)(n_i - n)(n_j - n),\qquad(2)$$

where n is the electron density (N_e/N, N_e electrons on a N-site cluster). Generically, we assume a screened Coulomb potential:

$$V(r) = V_0 \frac{\exp^{-r/\ell_0}}{r},\qquad(3)$$

where we will consider two typical values $\ell_0=2,4$ and $V_0 \in [0,5]$ and where the distance r is defined (to minimize finite-size effects) as the *periodized* distance on the torus.[22] The influence of this extra repulsive term in the competition between the *d*-wave RVB state and some inhomogeneous phases is quite subtle and will be discussed in the following.

To illustrate our future strategy, let us recall in more detail the simple basis of the RVB theory. It is based on a mean-field Hamiltonian which is of BCS type,

$$H_{BCS} = \sum_{\langle i,j\rangle,\sigma} (-\chi_0 c_{i\sigma}^\dagger c_{j\sigma} + \text{H.c.}) + \sum_{\langle i,j\rangle} (\Delta_{i,j} c_{i\uparrow}^\dagger c_{j\downarrow}^\dagger + \text{H.c.})$$
$$-\mu\sum_{i,\sigma} n_{i,\sigma},\qquad(4)$$

where χ_0 is a constant variational parameter, $\Delta_{i,j}$ is a nearest-neighbor *d*-wave pairing (with opposite signs on the vertical and horizontal bonds), and μ is the chemical potential. As a matter of fact, the BCS mean-field Hamiltonian can be obtained after a mean-field decoupling of the *t-J* model, where the decoupled exchange energy leads to the χ_0 and $\Delta_{i,j}$ order parameters. In this respect, we expect that the BCS wave function is a good starting point to approximate the ground state of the *t-J* model. However, such a wave function obviously does not fulfill the constraint of no-doubly occupied site (as in the *t-J* model). This can be easily achieved, at least at the formal level, by applying the full Gutzwiller operator[23] $\mathcal{P}_\mathcal{G}=\Pi_i(1-n_{i\uparrow}n_{i\downarrow})$ to the BCS wave function $|\psi_{BCS}\rangle$:

$$|\psi_{RVB}\rangle = \mathcal{P}_\mathcal{G}|\psi_{BCS}\rangle.\qquad(5)$$

The main difficulty to deal with projected wave functions is to treat correctly the Gutzwiller projection $\mathcal{P}_\mathcal{G}$. This can be done numerically using a conceptually exact variational Monte Carlo (VMC) technique[5–7] on large clusters. It has

been shown that the magnetic energy of the variational RVB state at half filling is very close to the best exact estimate for the Heisenberg model. Such a scheme also provides, at finite doping, a semiquantitative understanding of the phase diagram of the cuprate superconductors and of their experimental properties. Interesting results using a VMC technique associated to inhomogeneous wave functions will be presented in Sec. III.

Another route to deal with the Gutzwiller projection is to use a *renormalized mean-field (MF) theory*[24] in which the kinetic and superexchange energies are renormalized by different doping-dependent factors g_t and g_J, respectively. Further mean-field treatments of the interaction term can then be accomplished in the particle-particle (superconducting) channel. Crucial, now well established, experimental observations such as the existence of a pseudogap and nodal quasiparticles and the large renormalization of the Drude weight are remarkably well explained by this early MF RVB theory.[8] An extension of this approach[25,26] will be followed in Sec. II to investigate inhomogeneous structures with checkerboard patterns involving a decoupling in the particle-hole channel. As (re-)emphasized recently by Anderson and co-workers,[8] this general procedure, via the effective MF Hamiltonian, leads to a Slater determinant $|\Psi_{MF}\rangle$ from which a correlated wave function $\mathcal{P}_\mathcal{G}|\Psi_{MF}\rangle$ can be constructed and investigated by VMC. Since the MF approach offers a reliable *guide* to construct translational symmetry-breaking projected variational wave functions, we will present first the MF approach in Sec. II before the more involved VMC calculations in Sec. III.

II. GUTZWILLER-PROJECTED MEAN-FIELD THEORY

A. Gutzwiller approximation and mean-field equations

We start first with the simplest approach where the action of the Gutzwiller projector $\mathcal{P}_\mathcal{G}$ is approximately taken care of using a Gutzwiller approximation scheme.[23] We generalize the MF approach of Ref. 25 to allow for nonuniform site and bond densities. Recently, such a procedure was followed in Ref. 26 to determine under which conditions a 4×4 superstructure might be stable for hole doping close to 1/8. We extend this investigation to arbitrary small doping and other kinds of supercells. In particular, we shall also consider 45° tilted supercells such as $\sqrt{2}\times\sqrt{2}$, $\sqrt{8}\times\sqrt{8}$, and $\sqrt{32}\times\sqrt{32}$.

The weakly doped antiferromagnet is described here by the renormalized *t-J* model Hamiltonian,

$$H_{t-J}^{ren} = -tg_t\sum_{\langle ij\rangle\sigma} (c_{i,\sigma}^\dagger c_{j,\sigma} + \text{H.c.}) + Jg_J\sum_{\langle ij\rangle} \mathbf{S}_i\cdot\mathbf{S}_j,\qquad(6)$$

where the local constraints of no doubly occupied sites are replaced by statistical Gutzwiller weights $g_t=2x/(1+x)$ and $g_J=4/(1+x)^2$, where x is the hole doping. A typical value of $t/J=3$ is assumed hereafter.

Decoupling in both particle-hole and (singlet) particle-particle channels can be considered simultaneously leading to the following MF Hamiltonian:

$$H_{MF} = -t \sum_{\langle ij \rangle \sigma} g_{ij}^t (c_{i,\sigma}^\dagger c_{j,\sigma} + \text{H.c.}) + \sum_{i\sigma} \epsilon_i n_{i,\sigma}$$

$$-\frac{3}{4}J \sum_{\langle ij \rangle \sigma} g_{i,j}^J (\chi_{ji} c_{i,\sigma}^\dagger c_{j,\sigma} + \text{H.c.} - |\chi_{ij}|^2)$$

$$-\frac{3}{4}J \sum_{\langle ij \rangle \sigma} g_{i,j}^J (\Delta_{ji} c_{i,\sigma}^\dagger c_{j,-\sigma}^\dagger + \text{H.c.} - |\Delta_{ij}|^2), \quad (7)$$

where the previous Gutzwiller weights have been expressed in terms of local fugacities $z_i = 2x_i/(1+x_i)$ (x_i is the local hole density $1 - \langle n_i \rangle$), $g_{i,j}^t = \sqrt{z_i z_j}$, and $g_{i,j}^J = (2-z_i)(2-z_j)$, to allow for small nonuniform charge modulations.[27] The Bogoliubov–de Gennes self-consistency conditions are implemented as $\chi_{ji} = \langle c_{j,\sigma}^\dagger c_{i,\sigma} \rangle$ and $\Delta_{ji} = \langle c_{j,-\sigma} c_{i,\sigma} \rangle = \langle c_{i,-\sigma} c_{j,\sigma} \rangle$.

In principle, this MF treatment allows a description of modulated phases with *coexisting* superconducting order, namely supersolid phases. Previous investigations[26] failed to stabilize such phases in the case of the *pure* 2D square lattice (i.e., defect-free). Moreover, in this section, we will restrict ourselves to $\Delta_{ij} = 0$. The case where both Δ_{ij} and χ_{ij} are non-zero is left for a future work, where the effect of a defect, such as for instance a vortex, will be studied.

In the case of finite V_0, the on-site terms ϵ_i may vary spatially as $-\mu + e_i$, where μ is the chemical potential and e_i are on-site energies which are self-consistently given by

$$e_i = \sum_{j \neq i} V_{i,j} \langle n_j \rangle. \quad (8)$$

In that case, a constant $\sum_{i \neq j} V_{i,j}(\langle n_i \rangle \langle n_j \rangle + n^2)$ has to be added to the MF energy. Note that we assume here a *fixed* chemical potential μ. In a recent work,[28] additional degrees of freedom were assumed (for $V_0 = 0$) implementing an unconstrained minimization with respect to the on-site fugacities. However, we believe that the energy gain is too small to be really conclusive (certainly below the accuracy one can expect from such a simple MF approach). We argue that we can safely neglect the spatial variation of μ in first approximation, and this will be confirmed by the more accurate VMC calculations in Sec. III. Incidently, Ref. 28 emphasizes a deep connection between the stability of checkerboard structures[26] and the instability of the SFP due to nesting properties of some parts of its Fermi surface.[29]

B. Mean-field phase diagrams

In principle, the mean-field equations could be solved in real space on large clusters allowing for arbitrary modulations of the self-consistent parameters. In practice, such a procedure is not feasible since the number of degrees of freedom involved is too large. We therefore follow a different strategy. First, we assume fixed (square shaped) supercells and a given symmetry within the supercell (typically invariance under 90° rotations) to reduce substantially the number of parameters to optimize. Incidently, the assumed periodicity allows us to conveniently rewrite the mean-field equations in Fourier space using a reduced Brillouin zone with a very small mesh. In this way, we can converge to either an absolute or a local minimum. Therefore in a second step, the
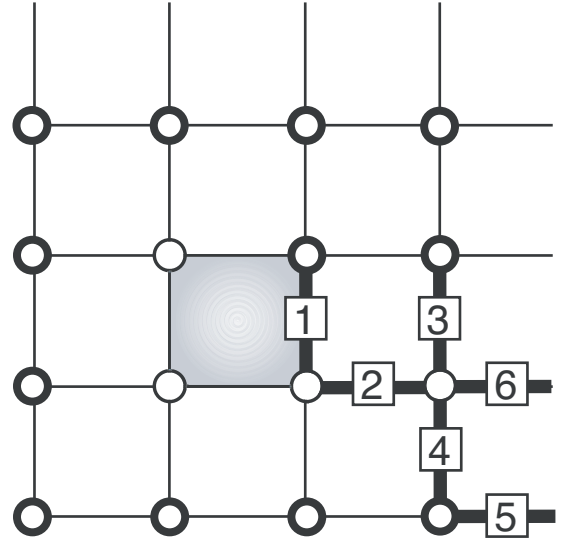

FIG. 1. (Color online) 4×4 unit cell used in both the MF approach and the variational wave function. Note the existence of six independent bonds (bold bonds), that for convenience are labeled from 1–6, and of three *a priori* nonequivalent sites. The center of the dashed plaquette is the center of the (assumed) C_{4V} symmetry. Other sizes of the same type of structure are considered in the MF case, respectively: 2×2, $\sqrt{8} \times \sqrt{8}$, and $\sqrt{32} \times \sqrt{32}$ unit cells.

MF energies of the various solutions are compared in order to draw an overall phase diagram.

In previous MF calculations,[26] stability of an inhomogeneous solution with the 4×4 unit cell shown in Fig. 1 was found around $x = 1/8$. Here, we investigate its stability for arbitrary doping and extend the calculation to another possible competing solution with a twice-larger (square) unit cell containing 32 sites. The general solutions with different phases and/or amplitudes on the independent links will be refered to as bond-order (BO) phases.[30] Motivated by experiments,[17,21] a C_{4V} symmetry of the inhomogeneous patterns around a central plaquette will again be assumed for both cases. Note that such a feature greatly reduces the number of variational parameters and hence speeds up the convergence of the MF equations. Starting from a central plaquette, like in Fig. 1, a larger $\sqrt{32} \times \sqrt{32}$ unit cell (not shown) can easily be constructed with ten nonequivalent bonds (with both independent real and imaginary parts) and *a priori* six nonequivalent sites. Note that this new unit-cell is now tilted by 45°.

At this point, it is important to realize that patterns with a smaller number of nonequivalent bonds or sites are in fact subsets of the more general modulated structures described above. For example, the SFP is obviously a special case of such patterns, where all the $\chi_{i,j}$ are equal in magnitude with a phase oriented to form staggered currents, and where all the sites are equivalent. This example clearly indicates that the actual structure obtained after full convergence of the MF equations could have *higher* symmetry than the one postulated in the initial configuration which assumes a random choice for all independent parameters. In particular, the equilibrium unit cell could be smaller than the original one and contain a fraction (1/2 or 1/4) of it. This fact is illustrated in
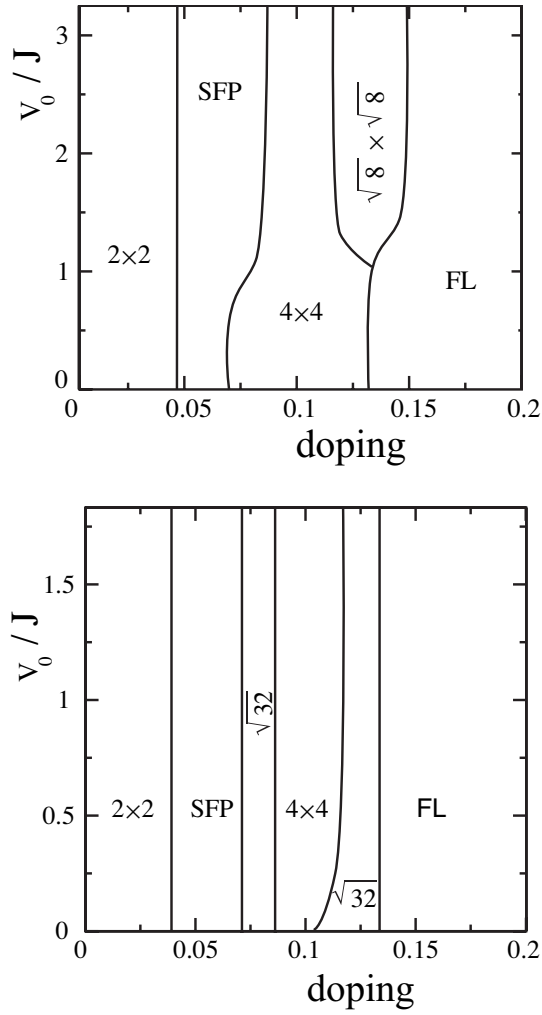
FIG. 2. Mean-field phase diagrams obtained by solving self-consistently the mean-field equations on a 128×128 lattice (for $\ell_0 = 4$) vs hole doping x and repulsion V_0 (in units of J). Top: results obtained assuming a 4×4 unit cell; bottom: the same with a $\sqrt{32} \times \sqrt{32}$ tilted unit cell. In both cases, a C_{4v} symmetry is assumed (see text).

Fig. 2 showing two phase diagrams produced by using different initial conditions, namely 4×4 (top) and $\sqrt{32} \times \sqrt{32}$ (bottom) unit cells. Both diagrams show consistently the emergence of the SFP at dopings around 6% and a *plaquette* phase (2×2 unit cell with two types of bonds) at very small doping.[31,32] In addition, a phase with a $\sqrt{8} \times \sqrt{8}$ supercell is obtained for a specific range of doping and V_0 (see Fig. 2 on the top). Interestingly enough, all these BO phases can be seen as *bond-modulated SFP* with 2, 4, 8 and up to 16 non-equivalent (staggered) plaquettes of slightly different amplitudes. This would be consistent with the SFP instability scenario[29] which suggests that the wave vector of the modulation should vary continuously with the doping. Although this picture might hold when $V_0 = 0$, our results show that the system prefers some peculiar spatial periodicities (like the ones investigated here) that definitely take place at moderate V_0.

Let us now compare the two phase diagrams. We find that, except in some doping regions, the various solutions ob-

tained with the 4×4 unit cell are recovered starting from a twice larger unit cell. Note that, due to the larger number of parameters, the minimization procedure starting from a larger unit cell explores a larger phase space and it is expected to be more likely to converge to the absolute minimum. This is particularly clear (although not always realized) at large doping $x = 0.14$, where we expect an homogeneous Fermi-liquid (FL) phase (all bonds are real and equal), as indeed seen in Fig. 2 on the bottom. On the contrary, Fig. 2 on the top reveals, for $V_0/J \in [1.5, 3]$, a modulated $\sqrt{8} \times \sqrt{8}$ structure, which is an artefact due to the presence of a local minimum (see next).

Since the MF procedure could accidentally give rise to local minima, it is of interest to compare the MF energies obtained by starting with *random* values of all independent parameters within the two previously discussed unit cells. For convenience, we have substracted from all data either the FL [in Fig. 3(a)] or the SFP [in Fig. 3(b)] *reference* energy. From Figs. 3(a) and 3(b) we see that we can converge towards a local-energy minimum, often modulated in space, which is not the absolute minimum. Indeed, over a large doping range, the lowest energy of all the solutions we have found is obtained for homogeneous densities and bond magnitudes. Nevertheless, we see that the 4×4 modulated phase is (i) locally stable and (ii) is very close in energy to the homogeneous (SFP) phase which, often, has a slightly lower energy. Note that, around $x \simeq 1/8$, the states with $\sqrt{8} \times \sqrt{8}$ and $\sqrt{32} \times \sqrt{32}$ supercells are clearly metastable solutions (and using a larger initial unit cell is not favorable in the latter case). In contrast, in this range of doping, the 4×4 checkerboard state is very competitive with respect to the SFP. Therefore it makes it a strong candidate to be realized either in the true ground state of the model, or present as a very low excited state.[33] In fact, considering such small energy differences, it is clear that an accurate comparison is beyond the accuracy of the MF approach. We therefore move to the *approximation-free* way of implementing the Gutzwiller projection with the VMC technique, that allows a detailed comparison between these variational homogeneous and inhomogeneous states.

III. VARIATIONAL MONTE CARLO SIMULATIONS OF 4×4 SUPERSTRUCTURES

Motivated by the previous mean-field results we have carried out extensive variational Monte Carlo simulations. In this approach, the action of the Gutzwiller projection operator is taken care of exactly, although one has to deal with finite clusters. In order to get rid of discontinuities in the d-wave RVB wave function, we consider (anti)periodic boundary conditions along e_y (e_x). As a matter of fact, it is also found that the energy is lower for twisted boundary conditions, hence confirming the relevance of this choice of boundaries. We have considered a 16×16 square cluster of $N = 256$ sites (unless specified otherwise). We also focus on the 1/8 doping case which corresponds here to $N_e = 224$ electrons on the 256-site cluster. Following the previous MF approach, we consider the same generic mean-field Hamiltonian,
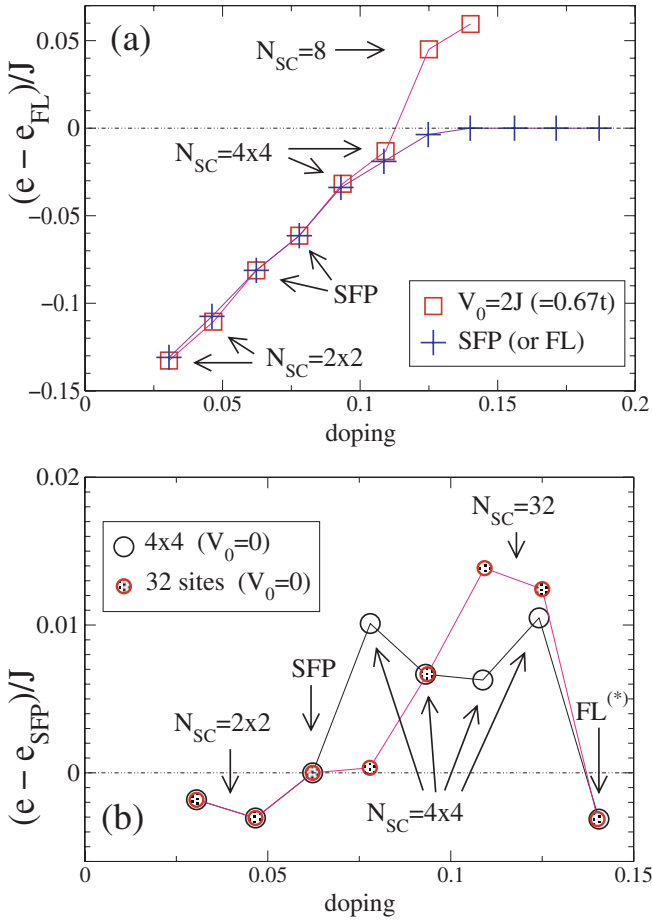
FIG. 3. (Color online) (a) Energy per site (in units of J and for $t=3J$) obtained by solving the mean-field equations using the *initial* 4×4 unit cell (see text) for a moderate value of V_0. The SFP energy is also shown for comparison. The FL energy has been substracted from all data for clarity. (b) Comparison of the energies (for $V_0=0$) using different initial conditions (see text), a 4×4 or a $\sqrt{32}\times\sqrt{32}$ unit cell; due to very small energy differences, the SFP energy is used as a reference for an easier comparison. The different phases specified by arrows and characterized by the number of sites N_{SC} of their actual supercells refer to the ones in Fig. 2. For doping $x=0.14$, the minimization leads to a solution with small imaginary parts (of order 10^{-4}) very similar to a FL phase, which we call FL*.

$$H_{MF} = \sum_{\langle i,j\rangle,\sigma} (-\tilde{t}_{i,j}c^{\dagger}_{i\sigma}c_{j\sigma} + \text{H.c.}) + \sum_{i\sigma} \epsilon_i c^{\dagger}_{i\sigma}c_{i\sigma}, \qquad (9)$$

where the complex bond amplitudes $\tilde{t}_{i,j}$ can be written as $|\tilde{t}_{i,j}|e^{i\theta_{i,j}}$, and $\theta_{i,j}$ is a phase oriented on the bond $i\rightarrow j$. The on-site terms ϵ_i allow to control the magnitude of the charge-density wave. However, the energy was found to be minimized for all the ϵ_i equal to the same value in the range $V_0=[0,5]$ and for the two parameters $\ell_0=2,4$. In fact, we find that strong charge-ordered wave functions are not stabilized in this model.[30]

In this section, we shall restrict ourselves to the 4×4 unit cell where all independent variational parameters are to be determined from an energy minimization. This is motivated both by experiments[17,21] and by the previous MF

TABLE I. Set of energies per lattice site for $V_0=1$ and $\ell_0=4$ for different wave functions. The best commensurate flux phase in the Landau gauge with flux per plaquette $p/16$ was found for $p=7$. We also show the energy of the CFP with flux $7/16$ written with another choice of gauge. We show the total energy per site (E_{tot}), the kinetic energy per site (E_T), the exchange energy per site (E_J), and the Coulomb energy per site (E_V).

Wave function	E_{tot}	E_T	E_J	E_V
FS	−0.4486(1)	−0.3193(1)	−0.1149(1)	−0.0144(1)
CFP 7/16[a]	−0.3500(1)	−0.1856(1)	−0.1429(1)	−0.0216(1)
CFP 7/16[b]	−0.4007(1)	−0.2369(1)	−0.1430(1)	−0.0208(1)
SFP	−0.4581(1)	−0.3106(1)	−0.1320(1)	−0.0155(1)
BO	−0.4490(1)	−0.3047(1)	−0.1302(1)	−0.0141(1)
RVB	−0.4564(1)	−0.3080(1)	−0.1439(1)	−0.0043(1)
SFP/$\mathcal{J}$	−0.4601(1)	−0.3116(1)	−0.1315(1)	−0.0169(1)
BO/$\mathcal{J}$	−0.4608(1)	−0.3096(1)	−0.1334(1)	−0.0177(1)
RVB/$\mathcal{J}$	−0.4644(1)	−0.3107(1)	−0.1440(1)	−0.0086(1)

[a]Landau gauge.
[b]Gauge of Ref. 16.

results showing the particular stability of such a structure (see also Ref. 26). As mentioned in the previous section, we also impose that the phases and amplitudes respect the C_{4V} symmetry within the unit cell (with respect to the center of the middle plaquette, see Fig. 1), reducing the numbers of independent links to 6. To avoid spurious degeneracies of the MF wave functions related to multiple choices of the filling of the discrete k vectors in the Brillouin zone (at the Fermi surface), we add very small random phases and amplitudes (10^{-6}) on all the links in the 4×4 unit cell.

Let us note that commensurate flux phase (CFP) are also a candidate for this special $1/8$ doping. In a previous study, a subtle choice of the phases $\theta_{i,j}$ (corresponding to a gauge choice in the corresponding Hofstadter problem[14]) was proposed,[16] which allows us to write the $\phi=p/16$ ($p<16$) flux per plaquette wave function within the same proposed unit cell[16] and is also expected to lead to a better kinetic energy than the Landau gauge (in the Landau gauge the unit cell would be a line of 16 sites). However, we have found that the CFP wave functions turned out *not* to be competitive for our set of parameters V_0, due to their quite poor kinetic energy, although they have very good Coulomb and exchange energies. We argue that such CFP wave functions would become relevant in the large Coulomb and/or J regimes (see Table I).

In order to further improve the energy, we also add a nearest-neighbor spin-independent Jastrow[34] term to the wave function,

$$\mathcal{P}_{\mathcal{J}} = \exp\left(\alpha \sum_{\langle i,j\rangle} n_i n_j\right), \qquad (10)$$

where α is an additional variational parameter. Finally, since the t-J model allows at most one fermion per site, we discard all configurations with doubly occupied sites by applying the

complete Gutzwiller projector $\mathcal{P}_G$. The wave function we use as an input to our variational study is therefore given by

$$|\psi_{\mathrm{var}}\rangle = \mathcal{P}_G \mathcal{P}_{\mathcal{J}} |\psi_{\mathrm{MF}}\rangle. \qquad (11)$$

In the following, we shall introduce simple notations for denoting the various variational wave functions, BO for the bond-order wave function, SFP for the staggered-flux phase, RVB for the d-wave RVB superconducting phase, FS for the simple projected Fermi sea, and we will use the notation MF/$\mathcal{J}$ (MF=BO, SFP, RVB, FS) when the Jastrow factor is applied on the mean-field wave function. Finally, it is also convenient to compare the energy of the different wave functions with respect to the energy of the simple projected Fermi sea (i.e., the correlated wave function corresponding to the previous FL mean-field phase), therefore we define a *condensation energy* as $e_c = e_{var} - e_{\mathrm{FS}}$.

In Fig. 4 we present the energies of the three wave functions BO/$\mathcal{J}$, SFP/$\mathcal{J}$, and RVB/$\mathcal{J}$ for Coulomb potential $V_0 \in [0,5]$. We find that for both $\ell_0 = 2$ and $\ell_0 = 4$ the RVB phase is not the best variational wave function when the Coulomb repulsion is strong. The bond-order wave function has a lower energy for $V_0 > 2$ and $\ell_0 = 2$ ($V_0 > 1.5$ and $\ell_0 = 4$). Note that the (short-range) Coulomb repulsion in the cuprates is expected to be comparable to the Hubbard U, and therefore $V_0 \approx 5$ or 10 seems realistic. Independently of the relative stability of both wave functions, the superconducting d-wave wave function itself is strongly destabilized by the Coulomb repulsion as indicated by the decrease of the variational gap parameter for increasing V_0 and the suppression of superconductivity at $V_0 \simeq 7$ (see Fig. 5).

Nevertheless, we observe that the difference in energy between the bond-order wave function and the staggered-flux phase is unexpectedly very small, although the two wave functions are quite different in nature. Indeed, we show in Table II the order parameters measured after the projection
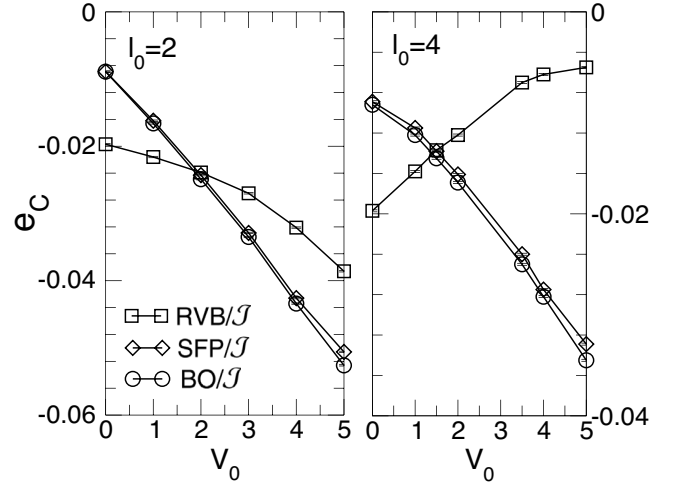

FIG. 4. Energy per lattice site of the RVB/$\mathcal{J}$, SFP/$\mathcal{J}$, and BO/$\mathcal{J}$ wave functions minus the energy of the projected Fermi-sea wave function.

for the RVB/$\mathcal{J}$, SFP/$\mathcal{J}$, and BO/$\mathcal{J}$ wave functions. We find that the RVB/$\mathcal{J}$ and the SFP/$\mathcal{J}$ wave functions are homogenous within the unit cell. In Fig. 6 we show the energy difference between the two wave functions. We found that the size dependance of the energy difference is rather small. Interestingly, the difference is increasing with the strength of the potential. We emphasize that the two wave functions correspond to two different local minima of the energy functional at zero Coulomb potential (see Fig. 7), which are very close in energy (the BO/$\mathcal{J}$ wave function is slightly lower in energy than the SFP/$\mathcal{J}$) and are separated by an energy barrier. Note that in Fig. 7 we consider the variational bond-order parameters and not the projected quantities.

Moreover, when the repulsion is switched on, the height of the energy barrier increases and the SFP/$\mathcal{J}$ wave function

TABLE II. Order parameters for the different wave functions for $V_0 = 1.5$ and $\ell_0 = 4$. We depict the following order parameters: $t_{i,j} \times e^{i\phi_{i,j}}$, where $t_{i,j}$ ($\phi_{i,j}$) is the amplitude (phase) of $\langle c_i^+ c_j \rangle$, and the exchange energy $\langle S_i \cdot S_j \rangle$, for the six independent bonds labeled for convenience according to Fig. 1. The sign of $\phi_{i,j}$ is according to the staggered-flux pattern (see arrows in Fig. 9). We note that the RVB/$\mathcal{J}$ is uniform by construction. The variational superconducting order parameter is $\Delta_{RVB} = 0.3$ for the RVB/$\mathcal{J}$ wave function and $\Delta_{RVB} = 0$ for the SFP/$\mathcal{J}$ and BO/$\mathcal{J}$ wave functions.

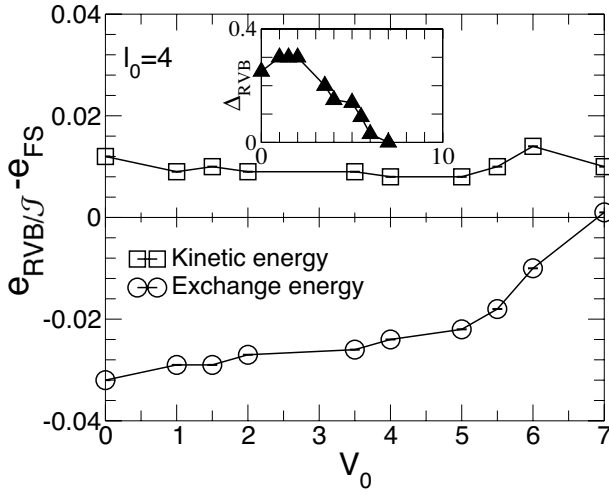|	Bond 1	Bond 2	Bond 3	Bond 4	Bond 5	Bond 6
$t_{i,j}$						
RVB/$\mathcal{J}$	0.077(1)	0.077(1)	0.077(1)	0.077(1)	0.077(1)	0.077(1)
SFP/$\mathcal{J}$	0.085(1)	0.085(1)	0.085(1)	0.085(1)	0.085(1)	0.085(1)
BO/$\mathcal{J}$	0.082(1)	0.083(1)	0.093(1)	0.088(1)	0.086(1)	0.084(1)
$|\phi_{i,j}|$						
RVB/$\mathcal{J}$	0	0	0	0	0	0
SFP/$\mathcal{J}$	0.438(1)	0.438(1)	0.438(1)	0.438(1)	0.438(1)	0.438(1)
BO/$\mathcal{J}$	0.527(1)	0.502(1)	0.473(1)	0.390(1)	0.338(1)	0.384(1)
$-\langle S_i \cdot S_j \rangle$						
RVB/$\mathcal{J}$	0.215(1)	0.215(1)	0.215(1)	0.215(1)	0.215(1)	0.215(1)
SFP/$\mathcal{J}$	0.197(1)	0.197(1)	0.197(1)	0.197(1)	0.197(1)	0.197(1)
BO/$\mathcal{J}$	0.215(1)	0.207(1)	0.215(1)	0.187(1)	0.186(1)	0.170(1)

FIG. 5. Kinetic and exchange energy per site of the RVB/$\mathcal{J}$ wave function minus the respective exchange and kinetic energy of the simple projected Fermi sea. Inset: value of the variational d-wave gap.

does not correspond anymore to the second local minima. Indeed, when $V_0 > 0$ the second local-energy minima *shifts* continuously from the point corresponding to the simple SFP/$\mathcal{J}$ wave function. The metastable wave function lying at this second local minima is a weak bond-order wave function that preserves a large kinetic energy while still being able to optimize its Coulomb energy better than the SFP. Moreover, to understand the striking difference of nature of the bond-order and staggered-flux wave functions, we have considered the difference in the respective kinetic energy, the exchange energy, and the Coulomb energy of the SFP/$\mathcal{J}$ and BO/$\mathcal{J}$ wave functions (see Fig. 8). We conclude that the two wave functions are qualitatively very different: the staggered-flux phase optimizes the kinetic energy whereas the bond-order wave function optimizes the Coulomb and exchange energies. Therefore we conclude that bond-order wave functions
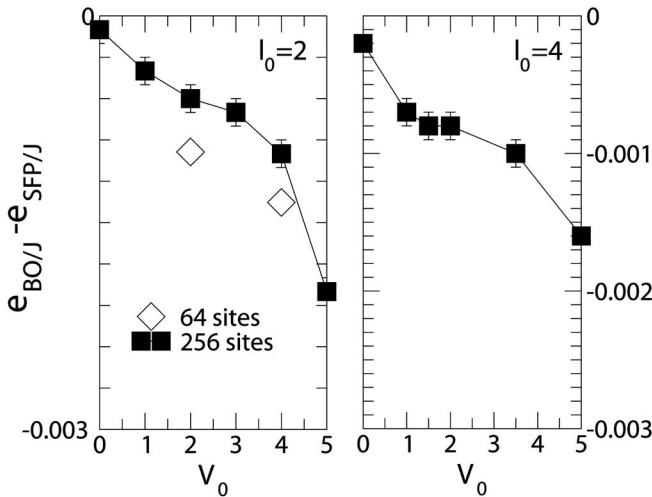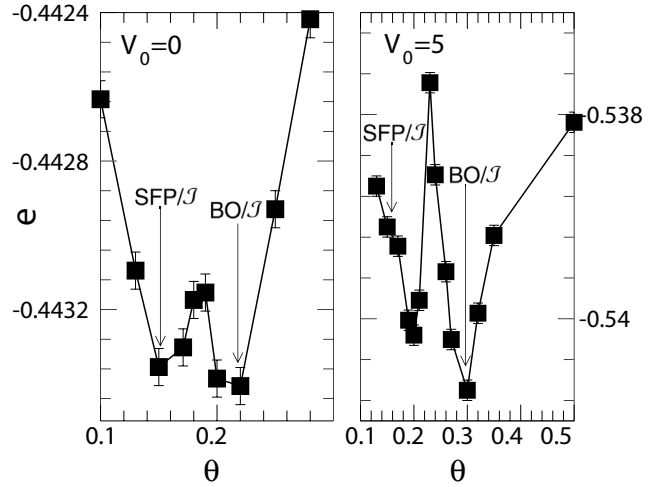

FIG. 7. Total energy per site of the BO/$\mathcal{J}$ variational wave function with variational parameters $\text{Im}(\tilde{t}_{i,j}) = \pm \theta$ on the bonds 1, 2, 3, and $\text{Im}(\tilde{t}_{i,j}) = \pm 0.149$ on the bonds 4, 5, 6. The sign of $\text{Im}(\tilde{t}_{i,j})$ is oriented according to the staggered flux pattern. We have chosen for all the links $\text{Re}(\tilde{t}_{i,j}) = 0.988$. Results for $V_0 = 0$ and $V_0 = 5$ with $\ell_0 = 4$ are shown.

are candidates to compete with the staggered-flux wave functions.

Finally, we emphasize that the bond-order wave function is not stabilized by the Coulomb repulsion alone (like for a usual electronic Wigner cristal) exhibiting coexisting bond order and (small) charge-density wave. Moreover, the variational parameters ϵ_i in Eq. (9) are found after minimizing the projected energy to be set to equal values on every site of the unit cell. Let us also emphasize that the bond-order wave function is not superconducting as proposed in some scenarios.[27] In the actual variational framework, we do not consider bond-order wave function embedded in a sea of d-wave spin singlet pairs.

In fact, we do not expect a bulk d-wave RVB state to be stable at large Coulomb repulsion (because of its very poor

FIG. 6. Total energy per site of the BO/$\mathcal{J}$ minus the energy of the SFP/$\mathcal{J}$ wave functions. For $\ell_0 = 2$ We show results for both lattices with 64 and 256 sites at the same 1/8 doping.
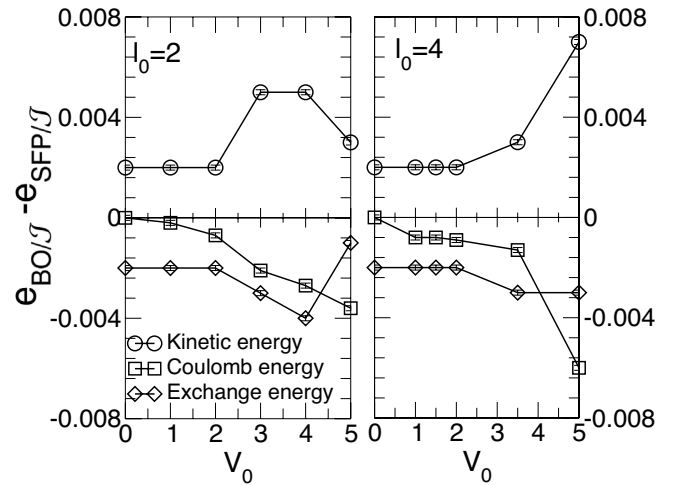

FIG. 8. Kinetic, exchange and Coulomb energy per site of the BO/$\mathcal{J}$ wave function minus the respective associated energy of the SFP/$\mathcal{J}$ wave function.
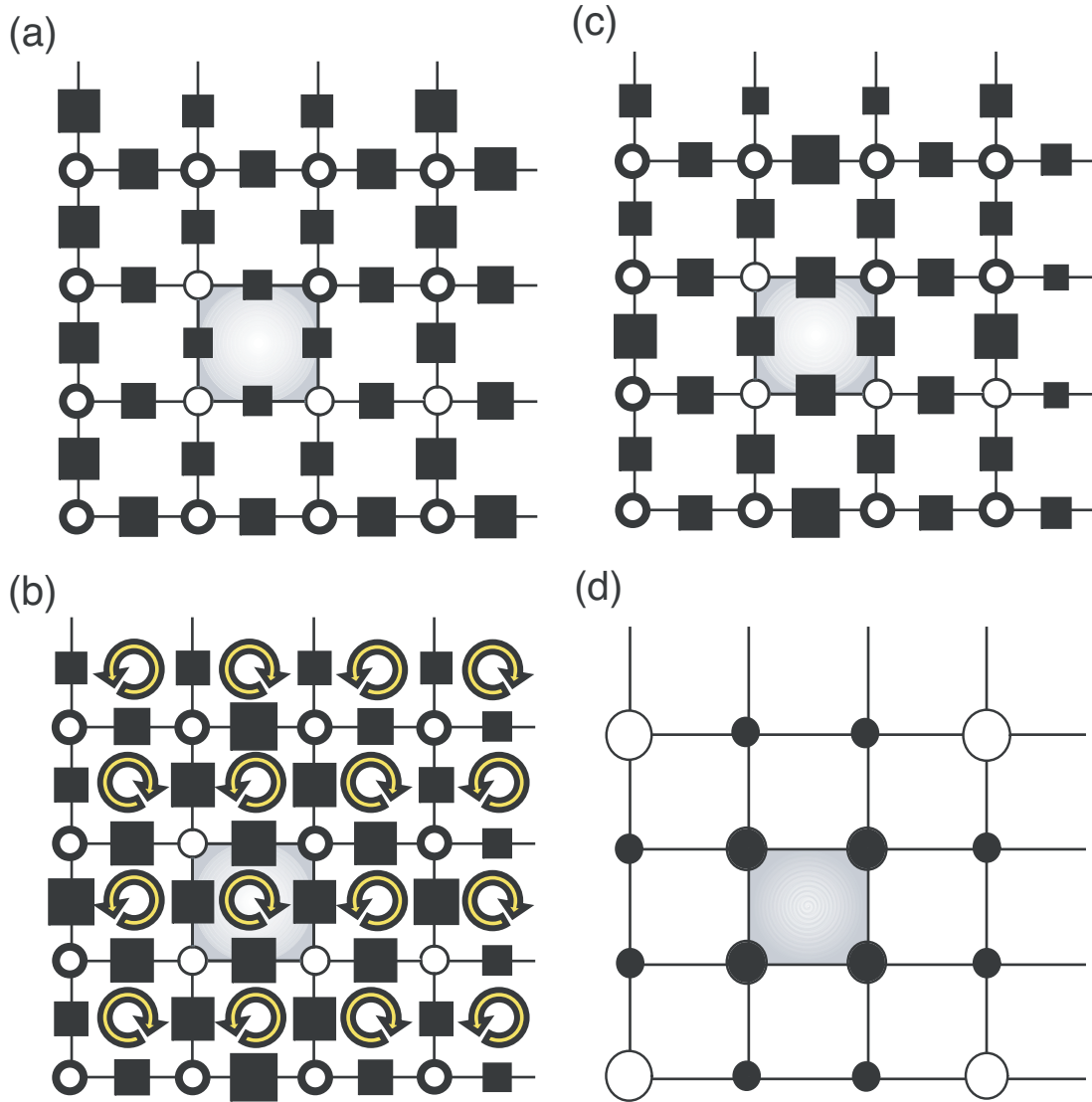
FIG. 9. (Color online) Local expectation values (a),(b),(c) of the kinetic and exchange energies of the projected BO/$\mathcal{J}$ wave functions on each of the bonds within the unit cell. Width of filled square symbols is proportional to the (a) real and (b) imaginary part of $\langle c_i^+ c_j \rangle$, and (c) to the local exchange energy $\langle \mathbf{S}_i \cdot \mathbf{S}_j \rangle$. The sign of the imaginary part of the hopping bonds is according to the staggered-flux pattern (arrows). The wave function has small charge-density variations (d), therefore we subtract the mean value n to the local density: size of circles are proportional to $\langle n_i - n \rangle$, and circles are open (filled) for negative (positive) sign. The biggest circle corresponds to an on-site charge deviation of 2%. All the above results are for $\ell_0 = 4$ and $V_0 = 5$.

Coulomb energy) nor a bulk *static* checkerboard phase at too small Coulomb energy. However, for moderate Coulomb repulsion for which the *d*-wave RVB remains globally stable, sizeable regions of checkerboard phase could be easily nucleated, e.g., by defects. This issue will be addressed using renormalized MF theory in a future work. An extension of our VMC study with simultaneous inhomogeneous bond-order and singlet pair order parameters (as required to treat such a problem) is difficult and also left for a future work. Note also that low-energy *dynamic fluctuations* of checkerboard character could also exist within the *d*-wave RVB state.

We present in Fig. 9 the real part and imaginary part of the measured hopping term $\langle c_i^+ c_j \rangle$ between every nearest-neighbor site of our candidate BO/$\mathcal{J}$ wave function. We also

present the exchange term on each bonds of the lattice, and the local on-site charge density. We find that the bond-order wave function has both (spin-spin) bond density wave and (small) charge-density wave components. Nonetheless, the charge modulations are very small (the maximum charge deviation from the mean on-site charge is of the order of 2%), and the charge density is a little bit larger in the center of the unit cell. As expected, the SFP/$\mathcal{J}$ has homogeneous hopping and exchange bonds within the unit cell. Therefore we conclude that after projection the two variational wave functions are very different in nature: the BO/$\mathcal{J}$ is strongly inhomogeneous for large Coulomb repulsion, but still preserving a competitive kinetic energy, and with very small charge modulation, whereas the SFP/$\mathcal{J}$ is totally homogeneous in space and optimize very efficiently the kinetic energy.

IV. CONCLUSION

In conclusion, in this work we have investigated the *t-J-V* model using both mean-field calculations as well as more involved variational Monte Carlo calculations. Both approaches have suggested that bond-order wave functions might be stabilized at zero and finite Coulomb repulsion for doping close to 1/8. In particular, variational Monte Carlo calculations show that a bond modulation appears spontaneously on top of the staggered-flux phase. This is in agreement with the work of Wang *et al.*[29] predicting an instability of the staggered flux. We have also shown that the modulated and homogeneous SFP, although nearby in parameter space, are, nevertheless, separated from each other by a small energy barrier. While both staggered-flux wave functions provide an optimal kinetic energy, the bond-modulated one exhibits a small extra gain of the exchange energy. On the other hand, a short-range Coulomb repulsion favors both staggered-flux wave function with respect to the *d*-wave RVB superconductors and brings them close in energy.

Clearly, the VMC studies rely on a specific ansatz and on physical intuitions on the physics of the microscopic model. However, we have chosen an enlarged parameter space so that, after optimization of the wave function containing an extended set of degrees of freedom, the result is expected to capture most of the physics of the *t-J-V* model. Second, the resulting wave function was shown to be very competitive with respect to extensively studied candidates such as the SFP and the *d*-wave RVB which are the usual ansatz to describe respectively the pseudogap and the superconducting phases of the *t-J* model. This wave function is definitively a good ansatz for more involved calculations, like Green-function Monte Carlo or Jastrow-like optimizations.

According to our results obtained in the *t-J-V* model with moderate Coulomb repulsion, only a weak charge modulation (2%) is observed while, however, a much more significant bond modulation is present (10%). It is at present stage difficult to estimate the effect of such a bond modulation in the local density of states (LDOS) and *a fortiori* in the STM signal. First, BOW are usually strongly coupled to the lattice (an effect not included here) and might affect the positions of the ions themselves. Second, we believe that a complete understanding of STM measurements in the presence of bond modulations is still missing and beyond the scope of our work. We argue, however, that both commensurate charge *and* bond modulations (which both are responsible for translation symmetry breaking) would participate to the superstructure peak in the LDOS, although a quantitative estimate is, so far, difficult to give.

Last, we would like to note that our wave function (or MF approach) is purely *static*. An extension including quantum fluctuations would be much more involved (although quite interesting) and it is difficult to estimate *a priori* the energy scales typical of such fluctuations. Further work is clearly needed on that front to, e.g., make the link with fluctuating orders in, e.g., Bi cuprates.

Finally, we suggest that the checkerboard pattern could spontaneously appear in the vicinity of a vortex in the mixed phase of the cuprates. Such an issue could be addressed by studying the *t-J-V* model on a square lattice extending our variational scheme to include *simultaneously* nearest-neighbor pairing and bond modulated staggered currents. It is expected that, while the pairing is suppressed in the vicinity of the vortex, the checkerboard pattern might be variationally stabilized in this region.

*Electronic address: didier.poilblanc@irsamc.ups-tlse.fr

[1] P. W. Anderson, Science **235**, 1196 (1987).

[2] F. C. Zhang and T. M. Rice, Phys. Rev. B **37**, 3759 (1988).

[3] E. Dagotto, Rev. Mod. Phys. **66**, 763 (1994).

[4] G. Kotliar, Phys. Rev. B **37**, 3664 (1988). This state can also be written as a projected *s+id* spin liquid.

[5] H. Yokoyama and H. Shiba, J. Phys. Soc. Jpn. **57**, 2482 (1988).

[6] C. Gros, Phys. Rev. B **38**, R931 (1988); for recent estimations see, e.g., A. Paramekanti, M. Randeria, and N. Trivedi, Phys. Rev. Lett. **87**, 217002 (2001).

[7] A. Paramekanti, M. Randeria, and N. Trivedi, Phys. Rev. B **70**, 054504 (2004).

[8] P. W. Anderson, P. A. Lee, M. Randeria, T. M. Rice, N. Trivedi, and F. C. Zhang, J. Phys.: Condens. Matter **16**, R755 (2004).

[9] I. Affleck and J. B. Marston, Phys. Rev. B **37**, R3774 (1988); J. B. Marston and I. Affleck, *ibid.* **39**, 11538 (1989).

[10] D. A. Ivanov, Phys. Rev. B **70**, 104503 (2004) and references therein; see also D. Poilblanc and Y. Hasegawa, *ibid.* **41**, 6989 (1990).

[11] P. A. Lee, N. Nagaosa, T. K. Ng, and X. G. Wen, Phys. Rev. B **57**, 6003 (1998).

[12] X. G. Wen and P. A. Lee, Phys. Rev. Lett. **76**, 503 (1996).

[13] M. U. Ubbens and P. A. Lee, Phys. Rev. B **46**, 8434 (1992).

[14] D. R. Hofstadter, Phys. Rev. B **14**, 2239 (1976).

[15] P. W. Anderson, B. S. Shastry, and D. Hristopulos, Phys. Rev. B **40**, 8939 (1989); D. Poilblanc, *ibid.* **40**, R7376 (1989); P. Lederer, D. Poilblanc, and T. M. Rice, Phys. Rev. Lett. **63**, 1519 (1989); for related results using slave boson MF techniques see, e.g., F. Nori, E. Abrahams, and G. T. Zimanyi, Phys. Rev. B **41**, R7277 (1990).

[16] D. Poilblanc, Y. Hasegawa, and T. M. Rice, Phys. Rev. B **41**, 1949 (1990).

[17] M. Vershinin, S. Misra, S. Ono, Y. Abe, Y. Ando, and A. Yazdani, Science **303**, 1995 (2004). Note that the first observation was made around a vortex core in J. E. Hoffman, E. W. Hudson, K. M. Lang, V. Madhavan, H. Eisaki, S. Uchida, and J. C. Davis,

ibid. **295**, 466 (2002).

[18] Note that the *energy-dependent* spatial modulations of the tunneling conductance of optimally doped BSCO can be understood in terms of elastic scattering of quasiparticles; see J. E. Hoffman, K. McElroy, D. H. Lee, K. M. Lang, H. Eisaki, S. Uchida, and J. C. Davis, Science **297**, 1148 (2002).

[19] G. Levy, M. Kugler, A. A. Manuel, O. Fischer, and M. Li, Phys. Rev. Lett. **95**, 257005 (2005).

[20] A. Hashimoto, N. Momono, M. Oda, and M. Ido, cond-mat/0512496 (unpublished).

[21] T. Hanaguri *et al.*, Nature (London) **430**, 1001 (2004).

[22] The Manhattan distance of Ref. 26 is used.

[23] M. C. Gutzwiller, Phys. Rev. Lett. **10**, 159 (1963); D. Vollhardt, Rev. Mod. Phys. **56**, 99 (1984).

[24] F. C. Zhang, C. Gros, T. M. Rice, and H. Shiba, Supercond. Sci. Technol. **1**, 36 (1988).

[25] D. Poilblanc, Phys. Rev. B **41**, R4827 (1990); note that, in this early treatment, uniform Gutzwiller parameters were assumed although the *phases* of the bond variables were allowed to vary spatially.

[26] D. Poilblanc, Phys. Rev. B **72**, 060508(R) (2005).

[27] Such a formulation should be appropriate as long as the deviations of $\langle n_i \rangle$ from the average density remain small. See P. W. Anderson, cond-mat/0406038 (unpublished); B. A. Bernevig *et al.*, cond-mat/0312573 (unpublished).

[28] C. Li, S. Zhou, and Z. Wang, Phys. Rev. B **73**, 060501(R) (2006).

[29] Z. Wang, G. Kotliar, and X. F. Wang, Phys. Rev. B **42**, R8690 (1990); note that the Fermi surface of the SFP is made of four small ellipticlike *pockets* centered around $(\pm\pi/2, \pm\pi/2)$.

[30] Note that the bond modulation itself leads to nonequivalent sites which, strictly speaking, should have slightly different electron densities (although the ϵ_i might be constant).

[31] Note that, in this regime, antiferromagnetism is expected. Such a competition is not considered here.

[32] Also found in $SU(2N)$ mean-field theory; see M. Vojta, Y. Zhang, and S. Sachdev, Phys. Rev. B **62**, 6721 (2000), and references therein.

[33] Our 4×4 solution bears some similarities with those obtained within $SU(2N)/Sp(2N)$ mean-field theories; see M. Vojta, Phys. Rev. B **66**, 104505 (2002). Note, however, that the large-N $Sp(2N)$ scheme implies a superconducting state.

[34] R. Jastrow, Phys. Rev. **98**, 1479 (1955).